

# Room-temperature optical detection of $^{14}\text{CO}_2$ below the natural abundance with two-color cavity ring-down spectroscopy

A. Daniel McCartt\* and Jun Jiang

*Center for Accelerator Mass Spectrometry, Lawrence Livermore National Laboratory,  
7000 East Avenue, Livermore, CA 94550, USA*

E-mail: mccartt1@llnl.gov

## Abstract

Radiocarbon's natural production, radiative decay, and isotopic rarity make it a unique tool to probe carbonaceous systems in the life and earth sciences. However, the difficulty of current radiocarbon ( $^{14}\text{C}$ ) detection methods limits scientific adoption. Here, two-color cavity ring-down spectroscopy detects  $^{14}\text{CO}_2$  in room-temperature samples with an accuracy of one-tenth the natural abundance in 3 minutes. The intra-cavity pump-probe measurement uses two cavity-enhanced lasers to cancel out cavity ring-down rate fluctuations and strong one-photon absorption interference ( $>10,000$  1/s) from hot-band transitions of  $\text{CO}_2$  isotopologues. Selective, room-temperature detection of small  $^{14}\text{CO}_2$  absorption signals ( $<1$  1/s) reduces the technical and operational burdens for cavity-enhanced measurements of radiocarbon, which can benefit a wide range of applications like biomedical research and field-detection of combusted fossil fuels.

LLNL-JRNL-831265

The history of a measured sample can be revealed by the presence of trace species within its constituents. Species with more unique provenance, rare abundance, or association with a particular phenomenon offer more unambiguous distinctions with their detection. One of the most famous trace species is radiocarbon ( $^{14}\text{C}$ ). It is a rare isotope of carbon (abundance  $1.2 \times 10^{-12}$   $^{14}\text{C}/\text{C}$ ), which is produced in the atmosphere by the interaction of cosmogenic neutrons with nitrogen and radiatively decays with a half-life of  $\sim 5700$  years.<sup>1,2</sup> These unique properties of radiocarbon can be leveraged for a wide variety of scientific applications (*e.g.*, radiocarbon dating, isotope tracer studies, cosmogenic nuclide analysis, etc.), but the rarity of  $^{14}\text{C}$  makes measurements challenging.<sup>3-5</sup> In the 1970s, nuclear physicist employed accelerator mass spectrometry (AMS) to increase the sensitivity of  $^{14}\text{C}$  detection. These room sized instruments utilized megavolt accelerators to separate  $^{14}\text{C}$  from its main interfering isobars ( $^{14}\text{N}$  and  $^{13}\text{CH}$ ) and achieved unprecedented sensitivity (*i.e.*,  $10^{-16}$   $^{14}\text{C}/\text{C}$ ).<sup>3,6</sup>

While  $^{14}\text{C}$  detection with AMS was initially developed for radiocarbon dating,  $^{14}\text{C}$ 's isotopic rarity in concert with AMS's sensitivity can track small quantities of  $^{14}\text{C}$ -labeled carbonaceous species through chemical systems. For example, the safety and efficacy of novel drugs can be tested in humans by administering  $^{14}\text{C}$ -labeled microdoses. These microdoses are small enough that they are not therapeutic, but  $^{14}\text{C}$ -tagged metabolites produced by the body can still be detected.<sup>4</sup>

The natural production and radiative decay properties of  $^{14}\text{C}$  provide opportunities to monitor the carbon cycle and fossil-fuel emissions.<sup>5,7,8</sup> Atmospheric  $\text{CO}_2$  is in constant flux with terrestrial and marine ecosystems at rates 20 times greater than human emissions. This makes the attribution of atmospheric  $\text{CO}_2$  measurements to emission point sources of combusted fossil fuels difficult and inaccurate. By measuring the dilution of atmospheric  $^{14}\text{CO}_2$  with combusted fossil fuels depleted of  $^{14}\text{C}$ , anthropogenic emissions can be monitored and differentiated from natural  $\text{CO}_2$  fluxes.<sup>7,8</sup> These atmospheric  $^{14}\text{CO}_2$  tracer measurements can verify "bottom-up" accounting estimates of fossil-fuel emissions and create a framework of accountability and trust for emission reduction agreements.<sup>9-11</sup> While scientists continue to

find new applications using  $^{14}\text{C}$ , the size, cost, and complexity of AMS limit these endeavors, particularly for high-throughput and fieldwork measurements.<sup>10–13</sup> This has spurred the development of alternative and more accessible means of  $^{14}\text{C}$  detection.

Cavity ring-down (CRD) spectroscopy has emerged as a viable  $^{14}\text{C}$  detection technique.<sup>14–20</sup> It utilizes strong anti-symmetric-stretch band ( $\nu_3$ ) transitions of  $^{14}\text{CO}_2$  in the mid-IR and has demonstrated parts-per-quadrillion (ppq) precisions ( $10^{-15}$   $^{14}\text{C}/\text{C}$ ), which are well below the natural abundance (*i.e.*,  $1.2 \times 10^{-12}$   $^{14}\text{C}/\text{C}$ ).<sup>16,17</sup> A high-finesse, optical cavity that is centimeters long can provide gas-laser interaction path lengths equivalent to kilometers. This cavity-enhanced path length increases the total gas absorption sensitivity, but this enhancement is not selective to the target analyte alone. Drifts in the cavity base loss and absorption interference from other species reduce the accuracy of traditional, cavity-enhanced techniques. Spurious reflections and external etalons coupled to the cavity cause frequency and time dependent undulations in the cavity base loss.<sup>21</sup> Drifts in these unwanted signals compromise traditional CRD trace gas measurements. Near the  $^{14}\text{CO}_2$   $\nu_3$  band in the Mid-IR, absorption interference is strong from  $\text{CO}_2$ -isotopologue hot-band transitions and other molecular species such as  $\text{N}_2\text{O}$ . Previous CRD measurements of  $^{14}\text{CO}_2$  with accuracy below the natural abundance mitigated against this interference by cooling the test gas.<sup>16–19</sup> However, the most accurate measurements cooled with two-stage refrigeration units, dry-ice baths, or Stirling engines, which negated the reduced size and portability benefits of laser based techniques. Even after cooling, the extremely weak  $^{14}\text{CO}_2$  signal had to be extracted from the dense interference (100 times smaller at natural abundance, 20 torr, and  $-20$  °C). This required laser wavelength scans and spectroscopic line-shape fitting of multiple overlapping features. While CRD has demonstrated  $^{14}\text{CO}_2$  sensitivities below the natural abundance which can be of service to multiple scientific fields, the difficulty of these measurements has largely confined them to laser spectroscopy laboratories.

Here, we present the first two-color, cavity ring-down spectroscopy (2C-CRDS) measurements of room-temperature  $^{14}\text{CO}_2$  samples. This recently developed intra-cavity pump-probe

technique uses an additional cavity-enhanced pump laser to selectively extract the signal of interest and cancel out instrument drift and unwanted background absorption interference.<sup>22</sup> Gas cooling and cavity-base-loss stabilization are no longer required for  $^{14}\text{CO}_2$  sensitivity. The burden of signal extraction is transferred from spectroscopic analysis to an intrinsic 2C-CRDS capability, and because of its noise cancelation, experimental conditions that would have been prohibitively unstable are now a possibility (*e.g.*, flow-through and field measurements). The unprocessed 2C-CRDS signal accurately detects  $^{14}\text{CO}_2$  concentrations with one tenth of the natural abundance. This is achieved in three minutes, at room temperature, and without spectral-fitting compensation for interfering species or cavity-base-loss variations.

These results exceed requirements for most biological and biomedical  $^{14}\text{C}$ -tracer experiments. However, as is evident by the 2C-CRDS precision with the cavity under vacuum (equivalent to 7‰ of the natural abundance, see supporting information), there is room for improving the 2C-CRDS measurement accuracy of  $^{14}\text{CO}_2$ . We determine precision from Allan deviation analysis that provides information about the stability of the 2C-CRDS signal during a single measurement. Accuracy is obtained from the mean absolute error of a linear fit to multiple sample types measured over a period of weeks. Factors that are contributing to the discrepancy between the demonstrated accuracy (91 ppq) and precision (33 ppq) are discussed, and spectroscopic strategies for overcoming this difference are presented. Improvements that bring the accuracy into line with the demonstrated precision would allow 2C-CRDS to address more demanding applications such as field measurements of fossil fuel emissions. This could transform existing “top-down” atmospheric  $\text{CO}_2$  monitoring systems to constrain “bottom-up” estimates of fossil fuel emissions, provide stakeholders with time and space resolved emissions data of both natural and fossil fuel derived  $\text{CO}_2$ , and create a platform of accountability and trust for national emission reduction commitments.

# Experimental

Figure 1 shows a schematic with the primary components of our 2C-CRDS setup and a three level diagram of the  $^{14}\text{CO}_2$  pump-probe scheme used in this paper. Two quantum cascade lasers (QCL) are injected into a high-finesse optical cavity in a counter propagating beam configuration. S- and p-polarization modes of the three-mirror, traveling-wave cavity share a common beam path but have different resonant cavity frequencies.<sup>23</sup> Using the Pound-Drever-Hall (PDH) technique, the pump laser is locked to a lower-finesse p mode ( $\mathcal{F}_p = 5280$ ) close to the  $^{14}\text{CO}_2$ ,  $\nu_3$ -band  $1 - 0$ , P(14) transition.<sup>24</sup> The probe laser is locked to a high-finesse s mode ( $\mathcal{F}_s = 67700$ ) near the  $\nu_3$ -band  $2 - 1$ , R(13) transition. Ring-down measurements are initiated by periodically interrupting the probe laser’s lock to the cavity. In between each ring-down event, the intra-cavity pump power is applied or removed by cycling the pump laser’s lock on and off. The difference between these “pump-on” and “pump-off” ring-downs provide a net, two-color signal sensitive to the pumped  $\nu_3 = 1$ ,  $J = 13$  population and compensated for instrument drift and one-color spectroscopic interference. Further details on the 2C-CRDS technique can be found in our previous paper on  $\text{N}_2\text{O}$ .<sup>22</sup>

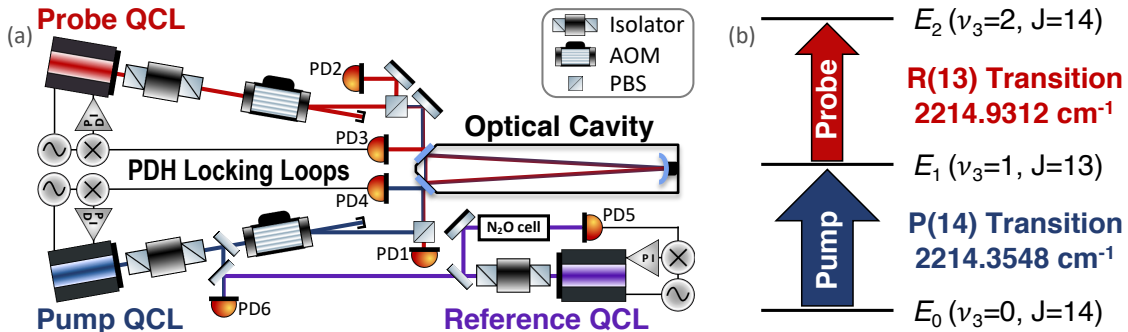


Figure 1: Summary of the experimental methods used for this study. A schematic of our 2C-CRDS experimental setup shown in panel (a), and the diagram of the ladder-type  $^{14}\text{CO}_2$  P(14)-R(13) pump-probe scheme is presented in panel (b). Both the pump (blue) and probe (red) QCLs are locked to the high-finesse optical cavity using PDH signals recorded at photo-detectors PD3 and PD4. The pump power is monitored with PD2 and ring-downs are recorded with PD1. Finally an additional reference QCL is locked to the  $\nu_3$   $1 - 0$ , R(16) transition of  $^{15}\text{N}^{14}\text{N}^{16}\text{O}$ . The beatnote between this laser and the pump recorded at PD6 provides a frequency reference for the 2C-CRDS experiments. PBS and AOM stand for polarization beam splitter and acousto-optic modulator.

The frequency spacings of the cavity resonant modes and the upper and lower molecular transitions influence the appearance of the intra-cavity two-color spectra.<sup>22</sup> The lasers are locked to a resonant mode of the cavity p- or s-polarization transmission “combs” and are simultaneously tuned when the cavity length is changed. Modes of a given polarization are separated by the cavity free spectral range ( $FSR$ ), and for a three-mirror cavity, the s and p “combs” are interleaved with a spacing of approximately half the  $FSR$ .<sup>23</sup> These experimental constraints of the cavity discretize the frequency-separation selection between the pump and probe lasers and when combined with the transition frequencies of the analyte, dictate the appearance and position of the intra-cavity two-color spectroscopic features.

Because of the high, intra-cavity, pump-laser power (17 W) and the counter-propagating beam configuration, 2C-CRDS measurements can exhibit several qualitatively different spectroscopic features. For  $^{14}\text{CO}_2$ , coherent, step-wise, and Autler-Townes-splitting features are observed with this experimental setup. The coherent features occur when the sum of the pump and probe laser frequencies is equal to the sum of the upper and lower molecular transition frequencies. These peaks are effectively Doppler-free as the near-identical frequencies of the counter propagating beams cancel out Doppler shifts from longitudinal velocities. The step-wise peaks are Doppler broadened and, unlike the coherent features, populate the intermediate  $\nu_3 = 1$  level during a two-step absorption process. Regardless of the pump detuning, step-wise peaks always occur at near-zero probe detuning. Finally, for features where both the pump and probe are near resonance, an Autler-Townes-type splitting is observed.<sup>25</sup>

## Results and Discussion

Figure 2 shows 2C-CRDS spectra of the  $^{14}\text{CO}_2$  1 – 0, P(14) and 2 – 1, R(13), intra-cavity, two-color transitions for a room-temperature, 4-torr, carbon-dioxide sample with 375 times the natural abundance of  $^{14}\text{C}$ . Three spectra from experiments where the pump and probe lasers were locked to different sets of cavity modes are plotted alongside simulations. The

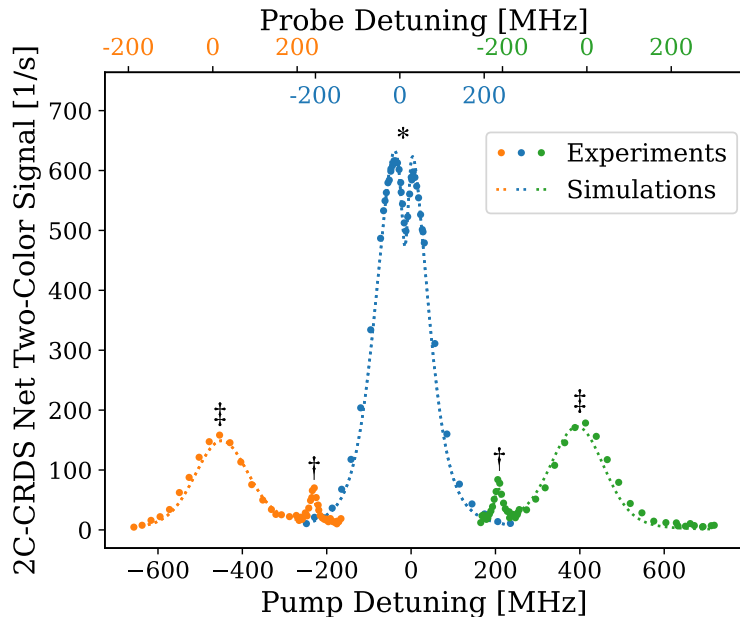


Figure 2: 2C-CRDS spectra of  $^{14}\text{CO}_2$  from combusted glucose with 375 times the natural abundance of  $^{14}\text{C}$ . Measurements were taken at room temperature and 4 torr. Note that the spectra are plotted against pump detuning on the lower axis, and the shifted probe detunings are shown on the color-coded upper axes for each of the three pump-probe spacings. Features are annotated with the following symbols: coherent †, step-wise ‡, Autler-Townes-type\*.

$^{14}\text{CO}_2$ , 2C-CRDS density matrix simulations are analogous to what was presented for our  $\text{N}_2\text{O}$  study.<sup>22</sup> Step-wise and coherent, two-color peaks were observed for experiments where the probe is locked to the mode on resonance with the  $^{14}\text{CO}_2$ , 2 – 1, R(13) probe transition and the pump was locked to a cavity mode detuned by one  $FSR$  (443 MHz or  $\sim 7$  times the Doppler half width) from the  $^{14}\text{CO}_2$ , 1 – 0, P(14) pump transition center frequency. When combined with a high-resolution measurement of the 1 – 0, P(14) transition,<sup>26</sup> the Doppler-free, coherent features provide an accurate quantification of the previously-unmeasured 2 – 1, R(13) transition wavenumber at  $2213.9319(3) \text{ cm}^{-1}$  (accuracy limited by the beat-note frequency reference). This is 0.017 and 0.014  $\text{cm}^{-1}$  greater than *ab initio* calculations for the 2 – 1, R(13) transition.<sup>27,28</sup> For this experiment’s cavity geometry, the  $^{14}\text{CO}_2$ , 1 – 0, P(14) and 2 – 1, R(13), transition-pair frequencies are separated by nearly an exact odd integer multiple of the discretized p- and s-mode frequency spacing (*i.e.*,  $\sim 57 \times FSR/2$ ). This allows the pump and probe lasers to be simultaneously tuned on resonance with their

respective transitions. In this case with the lower pump level of the ladder-type system driven by a large effective Rabi frequency ( $\sim 55$  MHz) and near identical pump and probe laser frequencies, the 2C-CRDS spectroscopic feature exhibits Autler-Townes-type splitting, which is well reproduced by the density matrix simulation.<sup>29,30</sup>

## Measurements of $^{14}\text{C}$ standards

2C-CRDS's  $^{14}\text{C}$  detection capabilities were characterized with  $\text{CO}_2$  samples from commercial sources and combusted " $^{14}\text{C}$  standards." Spectra were taken at room temperature and 20 torr (Figure 3a), and the  $^{14}\text{C}$  concentrations ranged from petrogenic ( $\sim$ zero  $^{14}\text{C}/\text{C}$ ) to approximately double the natural abundance (*i.e.*, 1.2 parts per trillion (ppt)  $^{14}\text{C}/\text{C}$ ). At 20 torr, the spectroscopic feature complexity is greatly reduced with the step-wise resonances dominating and the Autler-Townes-type effect minimized as a result of collisional broadening. 2C-CRDS resolves  $^{14}\text{CO}_2$  concentration differences that are fractions of the natural abundance in samples sourced from: petrogenic fuel (Petrogenic Cyl.), a 5240-year-old tree (TIRI Wood, *Pinus sylvestris*), 70-year-old cellulose (IAEA C3), contemporary corn (Biogenic Cyl.), and  $^{14}\text{C}$  elevated leaves collected near a medical waste facility (EBIS Leaves).<sup>31-35</sup> To demonstrate the detection selectivity of the 2C-CRDS method, the unprocessed two-color signal with the probe on resonance is compared with duplicate sample analysis by AMS (Figure 3b). Residuals from a linear fit of this comparison have a mean absolute error of 91 ppq—an accuracy that is better than 8% of the natural  $^{14}\text{C}$  abundance. Accuracy can be improved to 5% by averaging the results of each sample type and effectively increasing the averaging time. However, the rate of error reduction from averaging decreases after 3 minutes (see Figure S2). For the P(14)-R(13) pump-probe scheme and this set of samples, an elevated and varying background in the two-color signal (Figure 3a) is likely affecting averaging performance and this should be compensated or removed to increase the accuracy of 2C-CRDS  $^{14}\text{CO}_2$  detection.



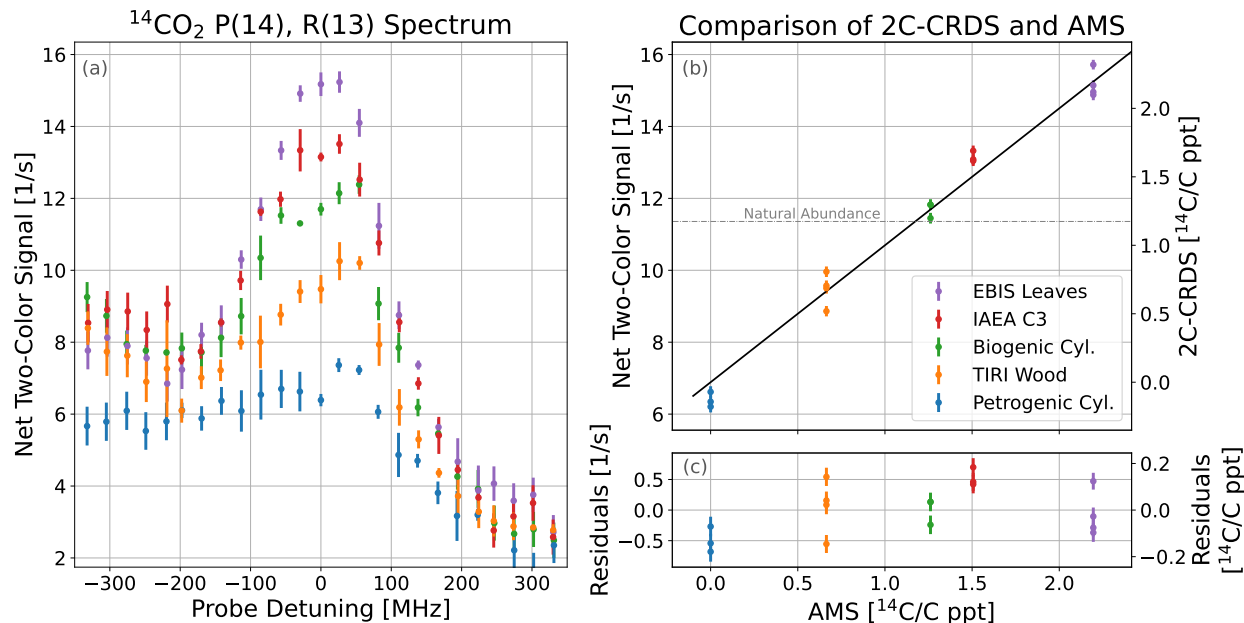


Figure 3: 2C-CRDS measurements of samples containing zero to two times the natural abundance of  $^{14}\text{C}$ . Panel (a) shows 2C-CRDS spectra averaged for a given sample type, and error bars represent the  $2 - \sigma$  standard deviation of these groupings. Panel (b) shows the comparison of 2C-CRDS measurements to AMS. The error bars are the 95% confidence interval for a single two-color measurement with the probe on resonance. A linear fit of the comparison is used to infer equivalent carbon-14 concentrations (axes on right), and the slope is constrained by a combusted glucose sample which contains 30 times the natural abundance of carbon-14 (not shown). The net two-color signal for a sample containing the natural abundance of  $^{14}\text{C}$  is indicated by a dash-dot style line. Panel (c) displays the residuals of the fit. The legend in panel (b) is for all three panels.

## Collisionally induced background

For the “ $^{14}\text{C}$ -standard” samples measured here, the one-color spectra are dominated by absorption interference from hot-band transitions of  $\text{CO}_2$  isotopologues. 2C-CRDS reduces this one-color interference by 3 orders of magnitude (Figure 4). However, additional two-color features are also present, which are contributing to the background at the  $^{14}\text{CO}_2$ , 2-1, R(13) probe frequency. At zero probe detuning, this background signal is similar in magnitude to the natural abundance  $^{14}\text{CO}_2$  signal (Figure 3a). Furthermore, off resonance (*e.g.*, -300 MHz probe detuning) there are statistically significant differences between samples in the background signal.

Like traditional pump-probe techniques, 2C-CRDS filters interfering transitions for species

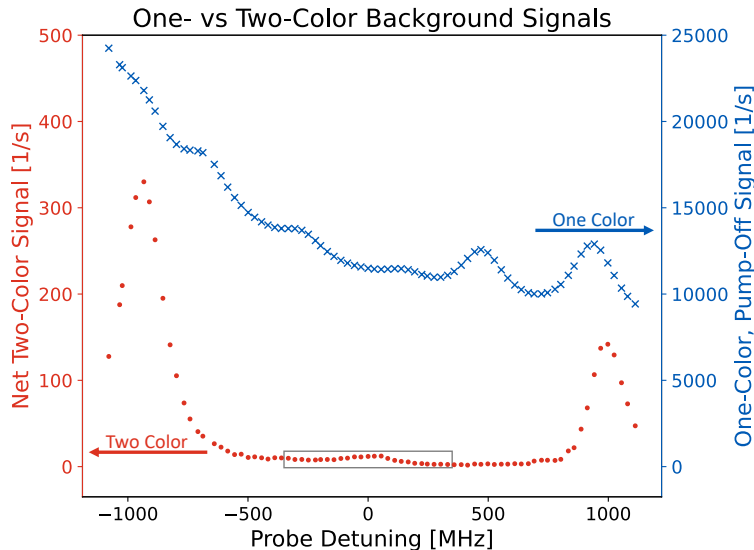


Figure 4: One- vs two-color background signals for the biogenic cylinder sample in the region surrounding the 2C-CRDS,  $^{14}\text{CO}_2$ ,  $1 - 0$  P(14),  $2 - 1$  R(13), two-color resonance. The net, two-color signal axis is on the left and the one-color signal axis is on the right. The grey rectangle surrounding some of two-color points delineates the area corresponding to the spectra shown for the “ $^{14}\text{C}$ -standards” (Figure 3a). While only probe detuning is indicated, the pump is scanned over an equivalent frequency range.

that are excited at both laser frequencies. This includes conventional quantum-state-linked transition pairs (*e.g.*,  $^{14}\text{CO}_2$   $1 - 0$ , P(14) and  $2 - 1$ , R(13)) but also collisionally induced two-color signals. The intense intra-cavity pump power can excite species with relatively far detuned transitions to vibrationally excited states. Populations are then redistributed to other vibrational and rotational states via collisions. For abundant species, even weak population transfer pathways from highly excited vibrational levels ( $\sim 5000 \text{ cm}^{-1}$  internal energy) can create signals significant to trace gas detection. Both *positive* and *negative* two-signals can occur depending on whether the pump-perturbed redistribution *increases* or *decreases* the probed state population. Inaccuracies from these unwanted two-color signals are exacerbated by their increased pump power dependence. Unlike the well saturated  $^{14}\text{CO}_2$  P(14) transition which has near zero pump detuning, the collisionally induced signals are likely pumped by relatively far detuned transitions and would be less saturated. Understanding the origin and variations of these background signals is important for maximizing the accuracy of 2C-CRDS detection, and we intend to conduct a more comprehensive study of the

system dynamics.

2C-CRDS was designed to cancel out cavity ring-down base-loss variations and spectroscopic interference, but the effect of some experimental parameters on the two-color dynamic system needs further characterization. For example, Allan deviation analysis of vacuum 2C-CRDS measurements has optimal averaging and a resultant precision of 0.03 [1/s] in 2.3 hours (supplementary text). When CO<sub>2</sub> is introduced into the cavity precision is only improved with averaging times up to 10 minutes (0.127 [1/s], 33 ppq <sup>14</sup>C/c). There is a clear correlation between the two-color signal and the intra-cavity pump power, and correcting for this variation with an empirically-determined, power-dependent model increases the time at which the minimum of the Allan deviation occurs. These pump power variation levels will not have an appreciable affect on the well saturated two-color <sup>14</sup>CO<sub>2</sub> signal (Figure S3), but they are likely causing significant variation in the two color background. The transmitted pump power drifted as the QCL thermally settled after power-up and with day-to-day changes in experimental conditions. Sample to sample pump power variation likely accounts for some of the two-color spread in Figure 3 and the discrepancy between the accuracy (91 ppq) and precision (33 ppq).

The selectivity of the uncompensated, room-temperature, two-color signal accurately detects a tenth of the natural <sup>14</sup>C abundance, which exceeds the requirements for nearly all <sup>14</sup>C-tracer applications in biology and medicine. 2C-CRDS development was funded to detect <sup>14</sup>C in biological samples separated by liquid chromatography (LC). Flow-through measurements have already been demonstrated in our earlier work.<sup>22</sup> This capability combined with its single frequency measurement selectivity should enable 2C-CRDS to make laser-based, in-line-flow-through measurements of <sup>14</sup>C in LC effluent.

To push the limits of 2C-CRDS <sup>14</sup>C detection, the small, two-color background variations must be addressed. While a model could be developed to compensate for variations in the P(14)-R(13) two-color background, there is likely another <sup>14</sup>CO<sub>2</sub> two-color line pair with less interference. In contrast to one-color measurements of <sup>14</sup>CO<sub>2</sub> that have a consensus

transition ( $\nu_3$  1–0, P(20)) and rely on further mitigation of determined interference to increase sensitivity (test-gas cooling, spectroscopic line shape fitting and compensation, etc.), 2C-CRDS still has many unmeasured two-color  $^{14}\text{CO}_2$  line pairs that could provide better opportunities for  $^{14}\text{C}$  detection. Within the tuning range of the QCL’s used in this study, P(14)-R(13) was the quantum-state-linked pair with the smallest two-color background, but collisionally induced signals can also be used for  $^{14}\text{CO}_2$  detection. A preliminary investigation using the collisionally-assisted 1–0, P(20) and 2–1, R(13) pump-probe scheme yields a reduced two-color background, and the  $^{14}\text{CO}_2$  signal is of similar strength to the linked two-color scheme used in this work due to facile rotational population relaxation within the  $\nu_3 = 1$  manifold. The inclusion of collisionally-assisted pump-probe schemes significantly increases  $^{14}\text{CO}_2$  two-color line-pair options and the likelihood of a set with reduced and stable background. After identifying the ideal line pair and constructing a model to compensate for any remaining two-color background signal, we are confident the accuracy of 2C-CRDS  $^{14}\text{CO}_2$  detection can be brought into line with the demonstrated precision.

While  $^{14}\text{CO}_2$  is a particularly demanding case study, 2C-CRDS can be applied to other species for trace-gas detection and quantum-state-resolved molecular spectroscopy. High-energy transitions, similar to those causing the interfering two-color background, are of interest to astrophysical observations. 2C-CRDS’s Doppler-free coherent resonances can accurately determine high-energy transition frequencies which are difficult to measure through thermal excitation and can be used to investigate the atmospheric composition of exoplanets.<sup>36–39</sup>

## Conclusion

2C-CRDS integrates the selectivity of pump-probe techniques with the sensitivity of cavity-enhanced detection. The resultant two-color spectrum focuses the sensitivity of the cavity on the species of interest and cancels out drift typical of cavity-enhanced instrumentation.

These qualities are ideal for trace-gas measurement. Furthermore, the pump-probe line-pair selection of 2C-CRDS affords experimental flexibility. 2C-CRDS can be tailored to compensate for interfering species prevalent in a given application and designed to maximize noise cancelation for field work. Careful study of the  $^{14}\text{C}$  two-color line-pair options and associated background signals is needed to realize the full  $^{14}\text{C}$  2C-CRDS detection potential, but the technique shows promise for atmospheric monitoring of anthropogenic  $\text{CO}_2$  emissions.  $^{14}\text{CO}_2$ 's utility for tracking fossil fuel emissions has been demonstrated on scales ranging from individual point sources to continents, and can provide an objective metric for coalitions of nations and municipalities that have agreed to reduce green-house-gas emissions.<sup>40,41</sup> 2C-CRDS's unique combination of sensitivity and field ability offer a logistically feasible and affordable means of consistently monitoring combusted fossil-fuel emissions with  $^{14}\text{CO}_2$ .

## Acknowledgement

The authors thank Professor Kevin K. Lehmann (UVA) and Dr. Davide Mazzotti (CNR-INO) for their thoughtful comments on the manuscript, and Ted Ognibene, Kari Finstad, Kurt Haack, Alexandra Hedgpeth, Caroline Stitt, and Esther Ubick (LLNL) for their assistance with the various samples.

Research reported in this publication was supported by the National Institute of General Medical Sciences of the National Institutes of Health (Award No. R01GM127573). The content is solely the responsibility of the authors and does not necessarily represent the official views of the National Institutes of Health. This work was performed, in part, at the National User Resource for Biological Accelerator Mass Spectrometry, which is operated at the LLNL under the auspices of the U.S. Department of Energy (Contract No. DE-AC52-07NA27344). The user resource was supported by the National Institutes of Health, National Institute of General Medical Sciences (Grant No. R24GM137748).

## Supporting Information Available

Additional experimental details, materials, and methods, supplementary text, including Figures S1, S2, and S3 (PDF)

## References

- (1) Libby, W. F. Atmospheric Helium Three and Radiocarbon from Cosmic Radiation. *Physical Review* **1946**, *69*, 671–672.
- (2) Kinsey, R. R.; Dunford, C. L.; Tuli, J. K.; Burrows, T. W. The NUDAT/PCNUDAT program for nuclear data (1996). 1996; <https://www.osti.gov/biblio/380330>, National Nuclear Data Center, information extracted from the NuDat 3.0 database (2021), <https://www.nndc.bnl.gov/nudat3/>.
- (3) Bennett, C. L.; Beukens, R. P.; Clover, M. R.; Gove, H. E.; Liebert, R. B.; Litherland, A. E.; Purser, K. H.; Sondheim, W. E. Radiocarbon Dating Using Electrostatic Accelerators: Negative Ions Provide the Key. *Science* **1977**, *198*, 508–510.
- (4) Turteltaub, K.; Vogel, J. Bioanalytical Applications of Accelerator Mass Spectrometry for Pharmaceutical Research. *Current Pharmaceutical Design* **2000**, *6*, 991–1007.
- (5) Heaton, T. J.; Bard, E.; Ramsey, C. B.; Butzin, M.; Köhler, P.; Muscheler, R.; Reimer, P. J.; Wacker, L. Radiocarbon: A key tracer for studying Earth’s dynamo, climate system, carbon cycle, and Sun. *Science* **2021**, *374*.
- (6) Nelson, D. E.; Korteling, R. G.; Stott, W. R. Carbon-14: Direct Detection at Natural Concentrations. *Science* **1977**, *198*, 507–508.
- (7) Levin, I.; Kromer, B.; Schmidt, M.; Sartorius, H. A novel approach for independent budgeting of fossil fuel CO<sub>2</sub> over Europe by <sup>14</sup>CO<sub>2</sub> observations. *Geophysical Research Letters* **2003**, *30*.

- (8) Turnbull, J.; Rayner, P.; Miller, J.; Naegler, T.; Ciais, P.; Cozic, A. On the use of  $^{14}\text{CO}_2$  as a tracer for fossil fuel  $\text{CO}_2$  : Quantifying uncertainties using an atmospheric transport model. *Journal of Geophysical Research* **2009**, *114*, D22302.
- (9) Lauvaux, T.; Gurney, K. R.; Miles, N. L.; Davis, K. J.; Richardson, S. J.; Deng, A.; Nathan, B. J.; Oda, T.; Wang, J. A.; Huttyra, L.; Turnbull, J. Policy-Relevant Assessment of Urban  $\text{CO}_2$  Emissions. *Environmental Science & Technology* **2020**, *54*, 10237–10245.
- (10) Miller, J. B.; Lehman, S. J.; Verhulst, K. R.; Miller, C. E.; Duren, R. M.; Yadav, V.; Newman, S.; Sloop, C. D. Large and seasonally varying biospheric  $\text{CO}_2$  fluxes in the Los Angeles megacity revealed by atmospheric radiocarbon. *Proceedings of the National Academy of Sciences* **2020**, *117*, 26681–26687.
- (11) Gurney, K. R.; Liang, J.; Roest, G.; Song, Y.; Mueller, K.; Lauvaux, T. Under-reporting of greenhouse gas emissions in U.S. cities. *Nature Communications* **2021**, *12*, 553.
- (12) Dell’Orco, S.; Christensen, E. D.; Iisa, K.; Starace, A. K.; Dutta, A.; Talmadge, M. S.; Magrini, K. A.; Mukarakate, C. Online Biogenic Carbon Analysis Enables Refineries to Reduce Carbon Footprint during Coprocessing Biomass- and Petroleum-Derived Liquids. *Analytical Chemistry* **2021**, *93*, 4351–4360.
- (13) Kratochwil, N. A.; Dueker, S. R.; Muri, D.; Senn, C.; Yoon, H.; Yu, B.-Y.; Lee, G.-H.; Dong, F.; Otteneder, M. B. Nanotracing and cavity-ring down spectroscopy: A new ultrasensitive approach in large molecule drug disposition studies. *PLOS ONE* **2018**, *13*, e0205435.
- (14) Genoud, G.; Vainio, M.; Phillips, H.; Dean, J.; Merimaa, M. Radiocarbon dioxide detection based on cavity ring-down spectroscopy and a quantum cascade laser. *Optics Letters* **2015**, *40*, 1342.

- (15) McCartt, A. D.; Ognibene, T.; Bench, G.; Turteltaub, K. Measurements of carbon-14 with cavity ring-down spectroscopy. *Nuclear Instruments and Methods in Physics Research Section B: Beam Interactions with Materials and Atoms* **2015**, *361*, 277–280.
- (16) Galli, I.; Bartalini, S.; Borri, S.; Cancio, P.; Mazzotti, D.; Natale, P. D.; Giusfredi, G. Molecular Gas Sensing Below Parts Per Trillion: Radiocarbon-Dioxide Optical Detection. *Physical Review Letters* **2011**, *107*, 270802, PRL.
- (17) Galli, I.; Bartalini, S.; Ballerini, R.; Barucci, M.; Cancio, P.; Pas, M. D.; Giusfredi, G.; Mazzotti, D.; Akikusa, N.; Natale, P. D. Spectroscopic detection of radiocarbon dioxide at parts-per-quadrillion sensitivity. *Optica* **2016**, *3*, 385.
- (18) McCartt, A. D.; Ognibene, T. J.; Bench, G.; Turteltaub, K. W. Quantifying Carbon-14 for Biology Using Cavity Ring-Down Spectroscopy. *Analytical Chemistry* **2016**, *88*, 8714–8719.
- (19) Fleisher, A. J.; Long, D. A.; Liu, Q.; Gameson, L.; Hodges, J. T. Optical Measurement of Radiocarbon below Unity Fraction Modern by Linear Absorption Spectroscopy. *The Journal of Physical Chemistry Letters* **2017**, *8*, 4550–4556.
- (20) Sonnenschein, V.; Terabayashi, R.; Tomita, H.; Kato, S.; Hayashi, N.; Takeda, S.; Jin, L.; Yamanaka, M.; Nishizawa, N.; Sato, A.; Yoshida, K.; Iguchi, T. A cavity ring-down spectrometer for study of biomedical radiocarbon-labeled samples. *Journal of Applied Physics* **2018**, *124*, 033101.
- (21) Huang, H.; Lehmann, K. K. Long-term stability in continuous wave cavity ringdown spectroscopy experiments. *Applied Optics* **2010**, *49*, 1378.
- (22) Jiang, J.; McCartt, A. D. Two-color, intracavity pump–probe, cavity ringdown spectroscopy. *The Journal of Chemical Physics* **2021**, *155*, 104201.



- (23) Saraf, S.; Byer, R. L.; King, P. J. High-extinction-ratio resonant cavity polarizer for quantum-optics measurements. *Applied Optics* **2007**, *46*, 3850.
- (24) Drever, R. W. P.; Hall, J. L.; Kowalski, F. V.; Hough, J.; Ford, G. M.; Munley, A. J.; Ward, H. Laser phase and frequency stabilization using an optical resonator. *Applied Physics B Photophysics and Laser Chemistry* **1983**, *31*, 97–105.
- (25) Autler, S. H.; Townes, C. H. Stark Effect in Rapidly Varying Fields. *Physical Review* **1955**, *100*, 703–722.
- (26) Galli, I.; Pastor, P. C.; Lonardo, G. D.; Fusina, L.; Giusfredi, G.; Mazzotti, D.; Tamassia, F.; Natale, P. D. The  $\nu_3$  band of  $^{14}\text{C}^{16}\text{O}_2$  molecule measured by optical-frequency-comb-assisted cavity ring-down spectroscopy. *Molecular Physics* **2011**, *109*, 2267–2272, Molecular Physics.
- (27) Zak, E. J.; Tennyson, J.; Polyansky, O. L.; Lodi, L.; Zobov, N. F.; Tashkun, S. A.; Perevalov, V. I. Room temperature line lists for CO<sub>2</sub> symmetric isotopologues with ab initio computed intensities. *Journal of Quantitative Spectroscopy and Radiative Transfer* **2017**, *189*, 267–280.
- (28) Huang, X.; Schwenke, D. W.; Freedman, R. S.; Lee, T. J. Ames-2016 line lists for 13 isotopologues of CO<sub>2</sub>: Updates, consistency, and remaining issues. *Journal of Quantitative Spectroscopy and Radiative Transfer* **2017**, *203*, 224–241.
- (29) Salomaa, R.; Stenholm, S. Two-photon spectroscopy. II. Effects of residual Doppler broadening. *Journal of Physics B: Atomic and Molecular Physics* **1976**, *9*, 1221–1235.
- (30) Lee, H.; Rostovtsev, Y.; Scully, M. O. Asymmetries between absorption and stimulated emission in driven three-level systems. *Physical Review A* **2000**, *62*, 063804.
- (31) Scott, E. M. Part 2: The Third International Radiocarbon Intercomparison (TIRI). *Radiocarbon* **2003**, *45*, 293–328.

- (32) Rozanski, K.; Stichler, W.; Gonfiantini, R.; Scott, E. M.; Beukens, R. P.; Kromer, B.; Plicht, J. V. D. The IAEA  $^{14}\text{C}$  Intercomparison Exercise 1990. *Radiocarbon* **1992**, *34*, 506–519.
- (33) Trumbore, S.; Gaudinski, J. B.; Hanson, P. J.; Southon, J. R. Quantifying ecosystem-atmosphere carbon exchange with a  $^{14}\text{C}$  label. *EOS, Transactions American Geophysical Union* **2002**, *83*, 265.
- (34) Swanston, C. W.; Torn, M. S.; Hanson, P. J.; Southon, J. R.; Garten, C. T.; Hanlon, E. M.; Ganio, L. Initial characterization of processes of soil carbon stabilization using forest stand-level radiocarbon enrichment. *Geoderma* **2005**, *128*, 52–62.
- (35) Hanson, P. J.; Swanston, C. W.; Garten, C. T.; Todd, D. E.; Trumbore, S. E. Reconciling Change in Oi-Horizon Carbon-14 with Mass Loss for an Oak Forest. *Soil Science Society of America Journal* **2005**, *69*, 1492–1502.
- (36) Foltynowicz, A.; Rutkowski, L.; Silander, I.; Johansson, A.; de Oliveira, V. S.; Axner, O.; Soboń, G.; Martynkien, T.; Mergo, P.; Lehmann, K. Sub-Doppler Double-Resonance Spectroscopy of Methane Using a Frequency Comb Probe. *Physical Review Letters* **2021**, *126*, 063001.
- (37) Showman, A. P. A whiff of methane. *Nature* **2008**, *452*, 296–297.
- (38) Guilluy, G.; Sozzetti, A.; Brogi, M.; Bonomo, A. S.; Giacobbe, P.; Claudi, R.; Benatti, S. Exoplanet atmospheres with GIANO. *Astronomy & Astrophysics* **2019**, *625*, A107.
- (39) Hu, C.-L.; Perevalov, V. I.; Cheng, C.-F.; Hua, T.-P.; Liu, A.-W.; Sun, Y. R.; Tan, Y.; Wang, J.; Hu, S.-M. Optical–Optical Double-Resonance Absorption Spectroscopy of Molecules with Kilohertz Accuracy. *The Journal of Physical Chemistry Letters* **2020**, *11*, 7843–7848.

- (40) Gurney, K. R.; Razlivanov, I.; Song, Y.; Zhou, Y.; Benes, B.; Abdul-Massih, M. Quantification of Fossil Fuel CO<sub>2</sub> Emissions on the Building/Street Scale for a Large U.S. City. *Environmental Science & Technology* **2012**, *46*, 12194–12202.
- (41) Basu, S.; Lehman, S. J.; Miller, J. B.; Andrews, A. E.; Sweeney, C.; Gurney, K. R.; Xu, X.; Southon, J.; Tans, P. P. Estimating US fossil fuel CO<sub>2</sub> emissions from measurements of <sup>14</sup>C in atmospheric CO<sub>2</sub>. *Proceedings of the National Academy of Sciences* **2020**, *117*, 13300–13307.

## *Supporting Information*

### **Room-temperature optical detection of $^{14}\text{CO}_2$ below the natural abundance with two-color cavity ring-down spectroscopy**

A. Daniel McCartt\* and Jun Jiang

*Center for Accelerator Mass Spectroscopy, Lawrence Livermore National Laboratory, 7000 East Avenue, Livermore, CA 94550, USA*

E-mail: [mccartt1@llnl.gov](mailto:mccartt1@llnl.gov)

This PDF file includes:

Materials and Methods

Supplementary Text

Figures S1, S2, and S3

# Materials and Methods

## <sup>14</sup>C Materials

The samples containing 30 and 375 times the natural abundance of <sup>14</sup>C are from dilutions of a combusted glucose mixture (Sigma G-5020 and Mallinckrodt 4912). The “Petrogenic Cylinder” sample is instrument grade CO<sub>2</sub> sourced from petroleum feedstock (Praxair). The “Biogenic Cylinder” sample is also instrument grade CO<sub>2</sub> but sourced from ethanol-based production using contemporary corn (~2015) as the feedstock (Airgas). The “TIRI Wood” sample is “Belfast Pine, Sample B” from the Third International Radiocarbon Intercomparison with designator Q7780.<sup>1</sup> “IAEA C3” is cellulose produced in 1989 from ~40 year old trees and used in the “The IAEA <sup>14</sup>C Intercomparison Exercise 1990”.<sup>2</sup> “EBIS Leaves” are from the “Enriched Background Isotope Study” and were collected near a medical waste facility that was emitting elevated levels of <sup>14</sup>C.<sup>3-5</sup>

## Sample Preparation

Duplicate samples containing up to 5 mg of carbon were aliquoted and dried under vacuum. These samples and approximately 150 mg of copper oxide were sealed in a quartz tubes using an acetylene torch. The tubes were then combusted at 900°C for 2 hours. Following combustion, AMS samples were graphitized and 2C-CRDS samples were transferred to the spectrometer front-end for purification. For 2C-CRDS sample purification, the quartz tubes were cracked under vacuum inside a bellows tube, and the sample gas was passed over an isopropanol/dry ice water trap. The gas was then exposed to a liquid nitrogen cold finger, and the gaseous species that remained were evacuated. The purified carbon dioxide was then introduced into the optical cavity.

## Details of the 2C-CRDS Method

The three-mirror, traveling-wave cavity, with total nominal round trip length of 66 cm, consists of two plano mirrors and a plano-concave mirror with 1-m radius of curvature (Lohn-Star). The two plano mirrors are glued directly onto an invar cavity spacer. The concave mirror is housed in a piezoelectric-transducer (PZT) assembly which is attached to the invar spacer. The laser incidence angle at the PZT mirror is  $\sim 1.5^\circ$ . The pump, probe, and reference lasers are continuous-wave (cw) distributed-feedback quantum cascade lasers (QCL) (Hamamatsu in high-heat-load packages). The pump (1000 mA maximum current) and probe (500 mA maximum current) lasers in the two-color, cavity ring-down experiments are each driven by a battery-powered QubeCL system from ppqSense, which provides low-noise electric current and temperature control. These lasers are modulated at 6 MHz. Light reflection off the cavity is measured with a HgCdTe (MCT) photodetector (Thorlabs PDAVJ8), and the MCT signal is demodulated with a frequency mixer (Mini-Circuit, ZRPD-1+). The resulting error signal is used as the input to the PID servo control loop (Vescent D2-125-PL) to achieve Pound-Drever-Hall laser frequency-locking to the cavity. The reference QCL is driven by a current controller from Wavelength Electronics (QCL500 Laboratory Series). The temperature of the reference QCL is regulated with a PI servo control loop (PTC2.5K-CH, Wavelength Electronics). The reference laser was modulated at 1.7 MHz. After a double pass through an optical cell (10 cm, 4.5 torr  $\text{N}_2\text{O}$ ) the transmitted intensity is recorded on an MCT photodetector (VIGO PVI-4TE-6/PIP-DC-20M) and the signal demodulated with a frequency mixer (Mini-Circuit, ZRPD-1+). Using wavelength modulation spectroscopy and the  $\nu_3$   $1 - 0$ , R(16) transition of  $^{15}\text{N}^{14}\text{N}^{16}\text{O}$  at  $2214.33886 \pm 0.001 \text{ cm}^{-1}$ , the reference laser is locked using a PI servo loop (New Focus LB1005).<sup>6</sup> The beatnote of the reference and pump lasers is recorded on an MCT detector (VIGO PVI-4TE-10.6/FIP-1k-1G) and provides frequency calibrations for the pump and probe lasers. The probe laser frequency is roughly measured using a wavemeter (Bristol 771) and then assigned a frequency using the beatnote and the cavity mode spacing. Timing for the experiment is provided with custom

code implemented on a field programmable gate array (NI PXIe-7976R, 5783). This system controls the AOMs (IntraAction Corp), provides corrections to the PDH servo integrators, and achieves ring-down rates greater than 2kHz.

For the “ $^{14}\text{C}$  standards” spectra, data acquisition was started with the cavity stabilized to zero probe detuning where ring downs were captured for 1000 seconds. To take the spectra, an additional 15 steps were measured for 100 seconds each. The cavity PZT was stepped using a feed-forward, pzt-creep-control profile in combination with closed-loop control from the frequency reference.<sup>7</sup>

## Supplementary Text

### Allan Deviation Analysis

In this paper, precision values represent the stability of the 2C-CRDS signal during the measurement of a single sample. Allan deviation analysis allows visualization and determination of this parameter.<sup>8,9</sup> Figure S1 shows the overlapping Allan deviation plots for the 2C-CRDS signal when measuring an empty cavity under vacuum, the “ $^{14}\text{C}$  standards”, and an elevated glucose sample containing 375 times the natural abundance of  $^{14}\text{C}$ . The fine grey lines are the Allan deviation analysis for each of the  $^{14}\text{CO}_2$  “standard” samples from Figure 3. The black points are the average of these  $^{14}\text{CO}_2$  “standard” samples’ individual Allan deviations calculated from the square root of the mean of the overlapping Allan variances. The orange points show the Allan deviation of the elevated glucose sample. We used a sample with the largest  $^{14}\text{CO}_2$  content to maximize the potential drift in the  $^{14}\text{CO}_2$  2C-CRDS signal. Finally, the blue data points are the Allan deviation of an empty cavity under vacuum. This is a measure of the maximum obtainable precision of the system for a given averaging time.

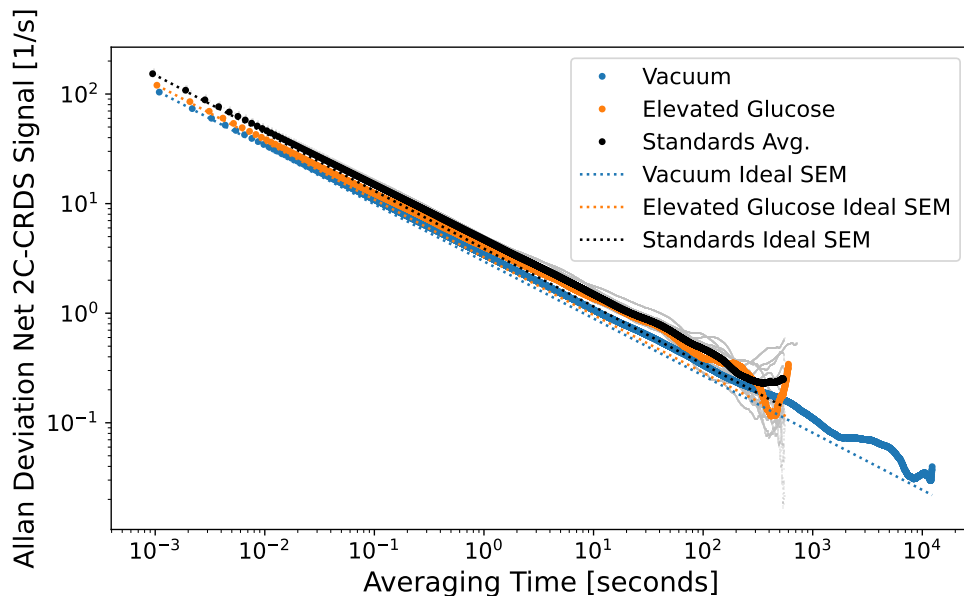


Figure S1. Allan deviation comparison of averaging stability for vacuum (blue),  $^{14}\text{C}$  “standards” (grey and their average black), and a  $\text{CO}_2$  sample with 375 times the natural  $^{14}\text{C}$  abundance (orange). Ideal averaging precision represented by the standard error of the mean (SEM) is indicated with dashed lines.

Dips in the Allan deviation below the *standard error of the mean* trend (*i.e.*,  $\sigma/\sqrt{N}$ ) represented by the dashed lines are likely non-physical representing a reversal of measurement drift and insufficient averaging time. For this reason, dips below the standard error of the mean trend seen in Figure S1 are corrected by taking the value at the intersection of the standard error of the mean trend and the Allan deviation turn around. This is a small and conservative correction. For example, this changes the reported elevated  $^{14}\text{CO}_2$  precision from 2.6% to 2.8% of the natural  $^{14}\text{C}$  abundance.

## Averaging Performance Analysis

Accuracy was determined by comparing 2C-CRDS and AMS measurements using a set of “ $^{14}\text{C}$  standards” (see the main manuscript). The residuals in Figure 3b have a mean absolute error (MAE) of 8%. Averaging over each sample type decreases this error to 5% by effectively increasing the measurement time to  $\sim 1$  hr. The rate of error reduction vs averaging time is visualized in Figure S2. The two-color signal for each sample type is concatenated and



divided into averaging windows of the plotted measurement time. The residuals are then calculated using the linear fit from Figure 3b.

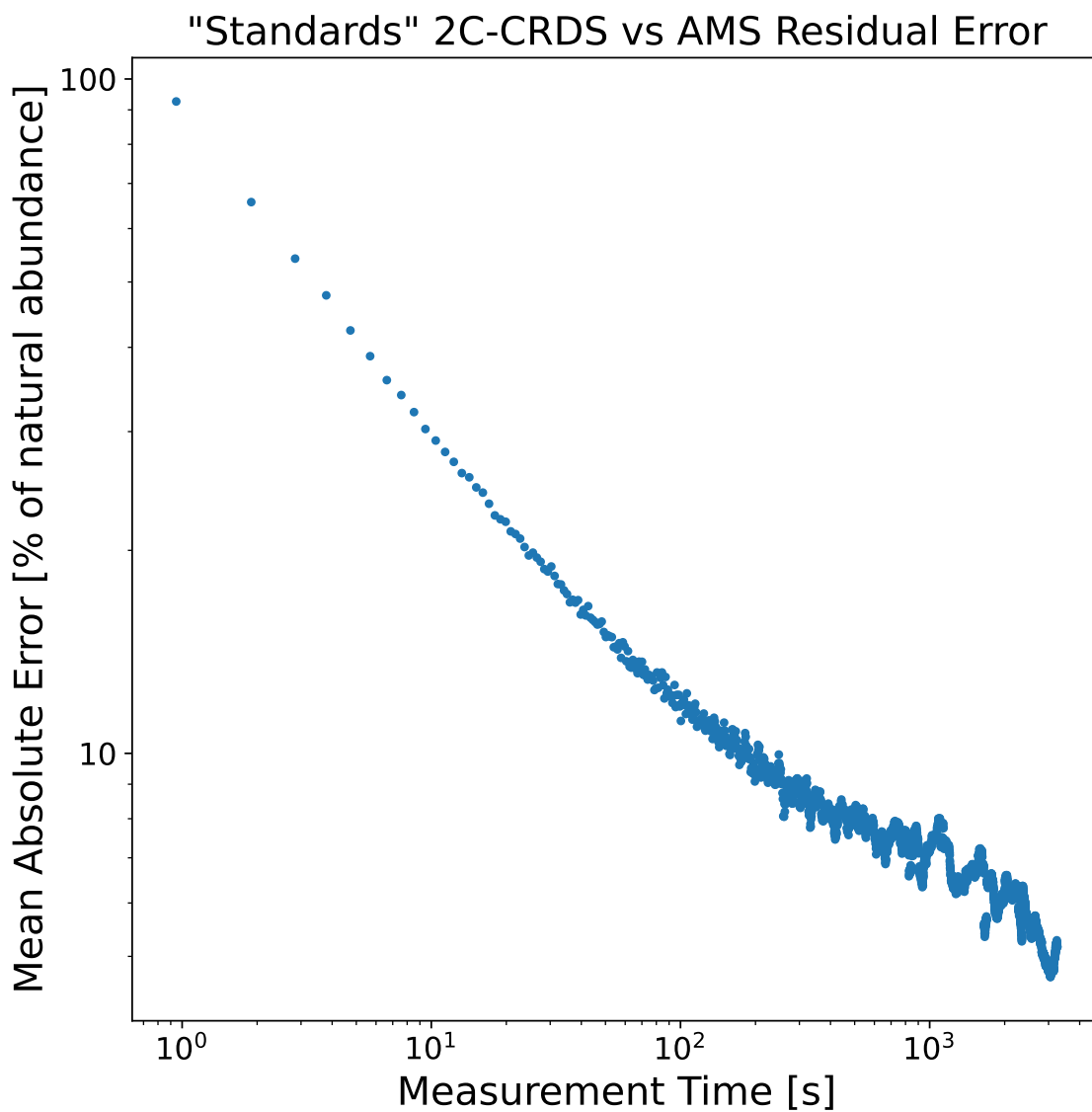


Figure S2. Analysis of “Standards” samples error reduction with averaging time.

## Two-Color Signal Pump Power Dependence

Figure S3 shows the pump-power dependence of the net two-color signal for a 22-torr carbon-dioxide sample with 375 times the natural abundance of <sup>14</sup>C. The net-two color signal is plotted vs the pump intensity transmitted through the cavity. For this sample, the net two-

color signal primarily originates from  $^{14}\text{CO}_2$  (>98%), and the signal is well saturated with half the applied intra-cavity pump power only reducing the net two color signal by 12%.

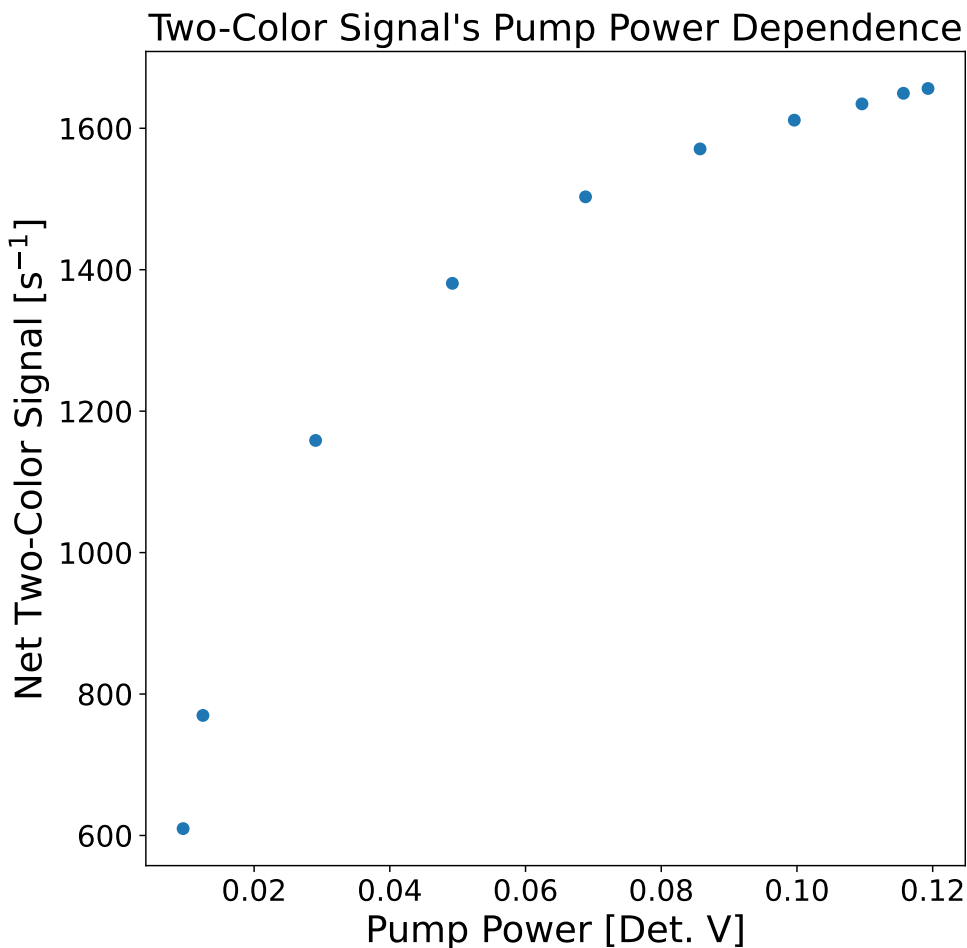


Figure S3. Pump power dependence of the net two-color signal for a 22 torr, carbon dioxide sample with 375 time the natural abundance of  $^{14}\text{C}$ . The net two-color signal is plotted versus detector voltage for the transmitted cavity pump beam.

## References

- (1) Scott, E. M. Part 2: The Third International Radiocarbon Intercomparison (TIRI). *Radiocarbon* **2003**, *45*, 293–328.
- (2) Rozanski, K.; Stichler, W.; Gonfiantini, R.; Scott, E. M.; Beukens, R. P.; Kromer, B.;

- Plicht, J. V. D. The IAEA  $^{14}\text{C}$  Intercomparison Exercise 1990. *Radiocarbon* **1992**, *34*, 506–519.
- (3) Trumbore, S.; Gaudinski, J. B.; Hanson, P. J.; Southon, J. R. Quantifying ecosystem-atmosphere carbon exchange with a  $^{14}\text{C}$  label. *EOS, Transactions American Geophysical Union* **2002**, *83*, 265.
- (4) Swanston, C. W.; Torn, M. S.; Hanson, P. J.; Southon, J. R.; Garten, C. T.; Hanlon, E. M.; Ganio, L. Initial characterization of processes of soil carbon stabilization using forest stand-level radiocarbon enrichment. *Geoderma* **2005**, *128*, 52–62.
- (5) Hanson, P. J.; Swanston, C. W.; Garten, C. T.; Todd, D. E.; Trumbore, S. E. Reconciling Change in Oi-Horizon Carbon-14 with Mass Loss for an Oak Forest. *Soil Science Society of America Journal* **2005**, *69*, 1492–1502.
- (6) Gordon, I. et al. The HITRAN2020 molecular spectroscopic database. *Journal of Quantitative Spectroscopy and Radiative Transfer* **2022**, *277*, 107949.
- (7) McCartt, A. D.; Ognibene, T. J.; Bench, G.; Turteltaub, K. W. Model-based, closed-loop control of PZT creep for cavity ring-down spectroscopy. *Measurement Science and Technology* **2014**, *25*, 095201.
- (8) Allan, D. Statistics of atomic frequency standards. *Proceedings of the IEEE* **1966**, *54*, 221–230.
- (9) Riley, W. J. *Handbook of frequency stability analysis*; 2008.